photonics

MDPI

Article

Nanotubes in Chitin Mode Locker for Passive Mode—Locked Fibre Laser in 2.0 μm Region

Nur Nadhirah Mohamad Rashid [1], Harith Ahmad [2], Mohammad Faizal Ismail [2], Muhammad Quisar Lokman [1], Siti Nur Fatin Zuikafly [1], Hafizal Yahaya [1], Nur Azmah Nordin [1], Wan Mohd Fazli Wan Nawawi [3] and Fauzan Ahmad [1,*]

[1] Malaysia-Japan International Institute of Technology (MJIIT), Universiti Teknologi Malaysia, Kuala Lumpur 54100, Malaysia
[2] Photonics Research Centre, University of Malaya, Kuala Lumpur 50603, Malaysia
[3] Department of Biotechnology Engineering, Kulliyyah of Engineering, International Islamic University Malaysia, Kuala Lumpur 50728, Malaysia
* Correspondence: fauzan.kl@utm.my

Abstract: This research demonstrated an ultrafast passively mode-locked thulium-holmium doped fibre laser (THDFL) using a carbon nanotube (CNT)-chitin composite film as a saturable absorber (SA). The CNTs were fabricated using ultrasonic-assisted liquid-phase exfoliation, and the chitin biopolymer was derived from oyster mushrooms (Pleurotus Ostreatus). The free-standing SA successfully performed a mode-locking operation at a threshold input pump power of 203 mW with an operating wavelength of 1908.53 nm. The generated mode-locked pulses had repetition rate, pulse width, and signal-to-noise ratio (SNR) values of 16 MHz, 1.1 ps, and 69 dB, respectively. The work demonstrates the potential of CNTs embedded in chitin biopolymer as a sustainable and environmentally friendly SA for a wide range of applications, particularly for pulsed lasers.

Keywords: saturable absorber; thulium-holmium doped fiber laser; carbon nanotubes; chitin

Citation: Mohamad Rashid, N.N.; Ahmad, H.; Ismail, M.F.; Lokman, M.Q.; Zuikafly, S.N.F.; Yahaya, H.; Nordin, N.A.; Wan Nawawi, W.M.F.; Ahmad, F. Nanotubes in Chitin Mode Locker for Passive Mode—Locked Fibre Laser in 2.0 μm Region. *Photonics* **2023**, *10*, 257. https://doi.org/10.3390/photonics10030257

Received: 7 February 2023
Revised: 24 February 2023
Accepted: 27 February 2023
Published: 28 February 2023

1. Introduction

Carbon nanotubes (CNTs) have been widely investigated and implemented as saturable absorbers (SA) for generating ultrashort pulses. This attention is due to the excellent properties of CNTs, including ultrafast recovery time, wide absorption bandwidth, high optical damage threshold, and ease of fabrication [1]. In the optical field in particular, CNTs are known for their direct bandgap properties, with the gap depending on the tube diameter [2,3]. Consequently, by growing nanotubes with the proper diameter distribution, it is possible to set absorption peak positions in a broad spectral range between visible and near-IR [4]. The first demonstration of a CNT-SA-based mode-locked erbium- doped fibre laser within this range was reported by Set et al. in 2003 [5]. They demonstrated a fibre laser with a picosecond (1 ps) pulse width in linear and ring configurations obtained by sandwiching SWCNTs between two optical plates. Since then, CNT-based mode-locked erbium-doped fibre lasers have been widely explored.

Recently the development of thulium-doped fibre lasers has been the subject of extensive research due to the high demand for extremely stable, low-cost, and ultrafast laser production in the mid-IR spectral region, in particular at 2 μm. This bandwidth offers a wide range of laser operating wavelengths in the eye-safe spectral region [6]. Thulium-doped laser sources operate in a wavelength range close to the absorption peaks of water molecules and most polycarbonate materials, making them appealing in many industrial applications, such as the biomedical and medical areas [7]. In comparison to holmium lasers, thulium lasers have a significant advantage in that Tm^{3+} ions can be directly stimulated with commercially available laser diodes of about 800 nm. Due to the limited availability of direct holmium-ion pumping sources, co-doping is the ideal strategy for

generating holmium-based fibre laser systems [8]. Co-doping with holmium ions enables energy transfer from the $3F^4$ state of thulium ions to the $5I^7$ state of holmium ions, which then generates lasing at wavelengths around 2 µm [9]. However, little has been reported on pulsed laser generation using this co-doped gain medium. In 2009, Kieu et al. [10] demonstrated a mode-locked thulium-holmium doped fibre (THDF) laser using a fibre taper embedded in an SWCNT–polymer composite. Two loop mirrors based on 2 × 2 fused couplers were incorporated into the fibre to form an optical cavity. The laser generated 750 fs soliton pulses with 0.5 nJ energy and 25 mW average power at a wavelength of ~1.9 µm [10]. Similarly, Kivistö et al. [11] studied the use of polymer-free CNTs on a highly reflective silver (Ag) mirror, which enabled the building of a robust and compact linear cavity laser. The THDF-doped fibre laser produced ~1.0 ps pulses with 15 mW average output power at the central wavelength of 1991 nm.

The incorporation of CNTs in laser cavities usually involves embedding the CNTs in synthetic polymers for ease of integration and removal, as well as for enhanced robustness and mechanical properties [12,13]. These synthetic polymers include PVA, PEO and PMMA, among others [14,15]. PVA, in particular, is a host polymer widely used for forming composites with materials such as MoS_2 [16], CNT [11,17], and graphene [18] owing to its high solubility in water, making the fabrication process easier while providing added strength without hindering the properties of the SA material itself. However, when PVA was used to form a composite with indium selenide, it resulted in higher optical loss and a reduction in transmittance from 92% to 86% [19]. PEO, a polymer alternative in optics, is also commonly used due to its desirable properties such as high thermal stability, mechanical flexibility, chemical stability, cost effectiveness, and excellent corrosion resistance [20–22]. However, the refractive index of this material is relatively low [23]. Bio-host polymers such as chitosan and chitin have been introduced as an alternative to synthetic polymers for producing a composite as an SA in the 2 µm region. However, chitosan can be harmful to human health [24], and therefore we used chitin as the host polymer for the fabrication of the CNT SA.

Chitin is the second most abundant natural polymer on earth after cellulose. It is found in the shells of crustaceans, insect exoskeletons, and fungi cell walls [25]. It has been used in many applications in areas such as the biomedical, nanotechnology, electronic, and solar cell industries due to its unique biochemical properties, such as biocompatibility, biodegradability, non-toxicity, and ability to form films [26,27]. Additionally, chitin is tough and durable in high-acidity and harmful environments, making it useful for producing films that can be used in high-power and high-temperature laser operations. This has been a problem for existing SAs, since the performance of the SA is often constrained by the host polymer's low heat resistance. This advantage has prompted the use of chitin in the fabrication of CNT-chitin-based SAs for pulsed laser generation [28]. Recently, Zuikafly et al. [28] used chitin as the host polymer in a graphene-based SA to generate a mode-locked pulsed fibre laser in the 2 µm region. The laser generated pulses with repetition rate and pulse width of 11.35 MHz and 7.033 ps, respectively. In contrast, this paper will discuss the performance of CNTs with a chitin-based SA in the mode-locking of a thulium-doped fibre laser operating in the 2 µm region.

2. Materials and Methods

2.1. Preparation and Characterisation of CNT–Chitin

The commercial CNTs used in the fabrication of this CNT–chitin were obtained from Cheap Tubes, Grafton, VT, USA (Length: 3–30 µm, purity: 99%) and were synthesized using catalytic chemical vapour deposition (CCVD). The CNTs consisted of an equal mix of SWCNT and double-walled carbon nanotubes (DWCNT) with inner diameters of 0.8–1.6 nm and 1–4 nm, respectively. Good preparation is needed to ensure a well-dispersed solution when mixing CNTs with a polymer, since the formation of CNT bundles in the polymer can obstruct the non-linear optical absorption due to the decrement of the optical Kerr effect, which is an important parameter for developing a good SA [2]. To "unzip" the

CNT bundles, we employed ultrasonic-assisted liquid phase exfoliation with the aid of sodium dodecyl sulphate (SDS) (Sigma Aldrich, Selangor, Malaysia). In the experiment, 1% of SDS was added to 400 mL of deionised (DI) water and stirred until completely dissolved. Then 250 mg of CNTs were added into the SDS solution and ultrasonically treated for 3 h using a probe sonicator (Q-Sonic) with output frequency and pulse amplitude of 20 kHz and 40%, respectively. During the ultrasonication, the pulse mode was set at 30 s on and 10 s off. Ultrasonication generates high local shear, specifically at the CNT bundle ends. When the bundle ends are "frayed" in this manner, the spaces between them become sites for SDS adsorption via hydrophobic interactions and Van der Waals forces. The SDS molecules gradually exfoliate the CNT bundles in an "unzippering" mechanism [29–33]. Subsequently the CNT suspension was centrifuged (Heraeus Multifuge X1, Thermo Scientific, Selangor, Malaysia) at 1000 rpm for an hour to allow for the sedimentation of agglomerated CNT bundles. The dispersed CNTs in the upper 20% of the solution in the centrifuge tube were carefully collected using a micropipette and transferred to a new centrifuge tube before mixing with the chitin polymer.

The preparation of the chitin polymer was performed following the procedure of Nawawi et al. (2019) [33]. *Pleurotus ostreatus* mushrooms were thawed and rinsed with distilled water for 5 min to remove any observable contaminants. After rinsing three times, the mushrooms were blended for 5 min using a commercial kitchen blender. An extraction process was performed using hot water at 85 °C for 30 min to remove any water-soluble components. Excess water containing soluble components was then removed by centrifugation, and the residual mushroom cake was soaked in 1 M NaOH to remove protein, lipid and alkaline-soluble polysaccharides, re-centrifuged to remove excess solids, and diluted in water (0.8% *w*/*v*) before being stored at 4 °C for further use. A pure chitin film was prepared by transferring the solution to a petri dish and leaving it to dry. To prepare the CNT-chitin SA, the CNT suspension was mixed with the chitin in a one-to-four ratio. The mixture was ultrasonicated for 60 min to ensure that the CNTs were evenly dispersed in the chitin. The mixture was then transferred to a petri dish and left to dry for 48 h at room temperature, resulting in a free-standing CNT-chitin-based SA film.

The fabricated CNT-chitin SA was characterized using transmission electron microscopy (TEM; JEOL, JEM-2100F, Tokyo, Japan) and field emission scanning electron microscopy (FESEM; JEOL, JSM-7800F, Tokyo, Japan) for morphological observation. The TEM analysis of the CNT-SDS in DI water was observed at a magnification of 20 nm and 5 nm, as shown in Figure 1a,b, which shows the tightly packed nanotube arrangement. Figure 1c shows the FESEM image of pristine CNT powder in bundled form. Without further sonication, the CNTs remain aggregated and the degree of dispersion is poor. Figure 1d shows the image of the CNT-chitin film. The CNTs are clearly well-dispersed within the matrices of the chitin fibrous structure.

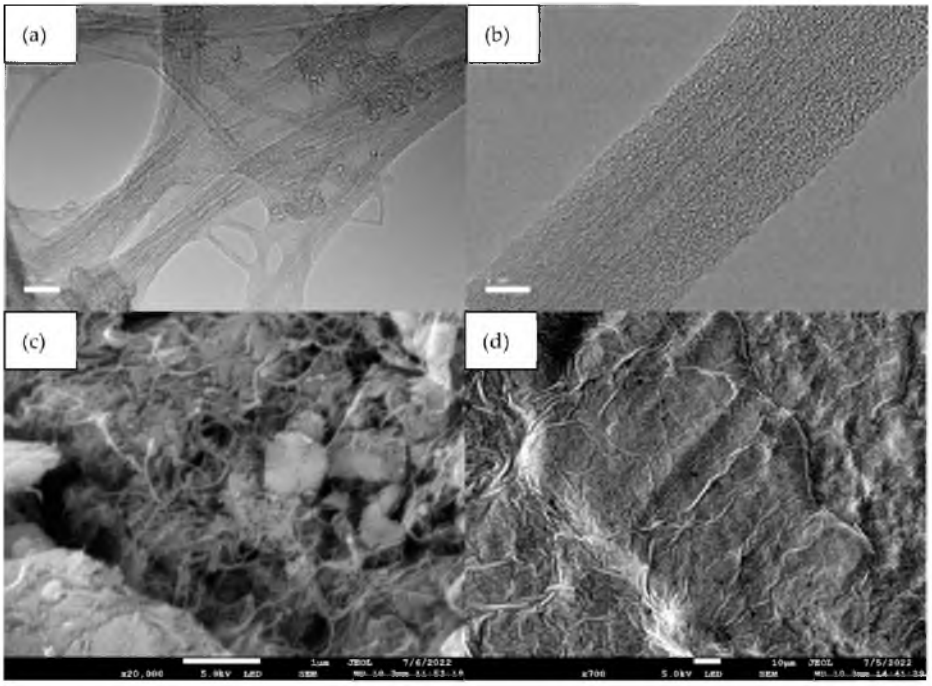

Figure 1. Surface morphology of CNT: (**a**,**b**) TEM images of CNT, (**c**) FESEM image of CNT powder, (**d**) FESEM image of CNT-chitin film.

Figure 2 shows the Raman spectrum representing the vibrational properties of the fabricated CNT-chitin, obtained via Raman spectroscopy (Alpha 300R, Witec, Ulm, Germany) through a 488 nm laser source at room temperature. Different vibrational bands were observed describing the characteristics of the CNTs. The characteristic Raman features of CNTs are seen in the radial breathing mode (RBM), which allows the estimation of the nanotubes' diameter with the following equation [34]:

$$\omega_{RBM} = \frac{A}{d_T} + B \tag{1}$$

where ω_{RBM} is the RBM frequency, d_T is the CNT diameter, $A = 248$ cm^{-1} and $B = 10$ cm^{-1}. In addition, several peaks in the RBM band are observed due to the inner and outer nanotubes and the interlayer interaction of the DWCNTs. In the RBM band, the peaks located at 152 cm^{-1} and 192 cm^{-1} represent the outer and inner layer of the DWCNTs [35]. By using the ω_{RBM} relation, the estimated nanotube diameters were found to be around 1.36 nm (inner) and 1.75 nm (outer), which are comparable with the CNT specification. Meanwhile, for the SWCNTs, the ω_{RBM} was observed to be between 120 cm^{-1} and 250 cm^{-1}, with the diameter ranging from 1 nm to 2 nm. It is our belief that the ω_{RBM} overlaps with the 152 cm^{-1} peak, based on a comparison with established Raman spectra of SWCNTs [34]. Defects and sp^3-hybridised carbon atoms give rise to a "D" band centered at 1354 cm^{-1}, the height of which is inversely related to nanotube quality [36]. The G-band comes from the graphite-like structure of the SWCNTs in the 2D plane mode. The spectrum clearly shows the distinct feature of the SWCNTs in which the so-called G peak, which originates from the tangential vibrations of the carbon atoms [37], is observed to be prominent at 1593 cm^{-1}. The sharp Lorentzian G peak indicates that the semiconducting SWCNTs have been properly deposited on the fibre ferrule end [38]. There is a resonant 2D peak at 2600 cm^{-1} occurring as an overtone of the "D" band [36].

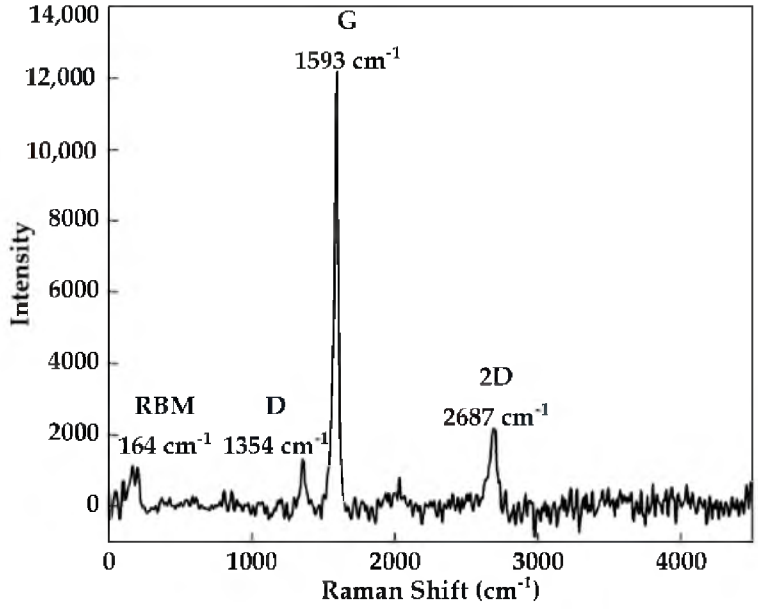

Figure 2. Raman spectrum of CNT-chitin film.

2.2. Determination of Linear and Non-Linear Optical Properties of CNT–Chitin Saturable Absorber

Prior to the insertion of the CNT-chitin SA in the laser cavity, linear and non-linear measurement was performed to optically characterize the CNT-chitin. The linear measurement was performed using a UV-Vis-NIR spectrophotometer (Lambda 750, Pelkin Elmer, Waltham, MA, USA) in which two samples, chitin and CNT-chitin with thickness of around 50 μm, were carefully inserted in the transmission sample holder to ensure that the film position was fixed during measurement. Figure 3a shows the linear optical transmission spectrum, which extends from 1000 nm to 2500 nm. The result shows that the transmission spectra of the CNT-chitin and pure chitin were around 24% and 78%, respectively, at a wavelength of 2000 nm. The presence of CNTs reduces transparency and absorbs light more than that of the host polymer [39,40], which in this case was pure chitin. The mechanism of the saturable absorber is based on the light absorbance of the material, and therefore attenuates high-intensity light at a specific wavelength [1]. This explains why chitin on its own cannot be used as a saturable absorber for generating light pulses. The addition of CNTs reduces transmission while increasing absorbance, making CNT-chitin a feasible SA in the 2 μm region [41,42]. The transmission spectrum in Figure 3a has features similar to those reported by Cheng et al. [43] due to the presence of DWCNTs. The DWCNTs provide strong absorption in the E_{11} and E_{22} bands where the inner nanotubes are responsible for E_{11} absorption at ≈1000 nm and the outer nanotubes are responsible for E_{11} absorption at ≈2000 nm and E_{22} absorption at ≈1000 nm [44]. Hasan et al. [45] mentions that the strong E_{11} and E_{22} absorption is related to the DWCNT inner and outer nanotube diameters, from 0.8–1.1 nm and 1.6–1.8 nm, respectively. Interestingly, the outer diameter of the DWCNTs in our experiment ranges from 1.0 to 4.0 nm, which is practical for mode-locked generation in the 2000 nm region. It is noted that the optical transmission spectrum shown in Figure 3a is linear compared to reference [42], whereas the optical transmission of CNT is not purely linear in the range of 1000 nm to 2000 nm. There are several reasons for this difference in the transmission spectrum as compared to the reference [42]. Unless samples with exactly the same composition, concentration, distribution and thickness are used, it is likely that a different transmission spectrum will be obtained. A shift in transmission spectrum is possible, as different molecules and compounds absorb light at different wavelengths. This applies to the difference in composition and concentration, since it also leads to a change in the amount of light absorbed [46]. Furthermore, there are several other factors to be taken into consideration, including the effect of surfactant during the fabrication process and

environmental factors such as humidity, pressure, and exposure to radiation during the measurement of the transmission spectrum [47,48]. Figure 3b shows the optical bandgap energy determined using the Tauc relation. The result shows that the bandgap energy for the CNTs was around 0.6 eV, corresponding to the diameter of the CNTs used in this work, which is suitable for operations in the 1000 to 2000 nm wavelength range [45].

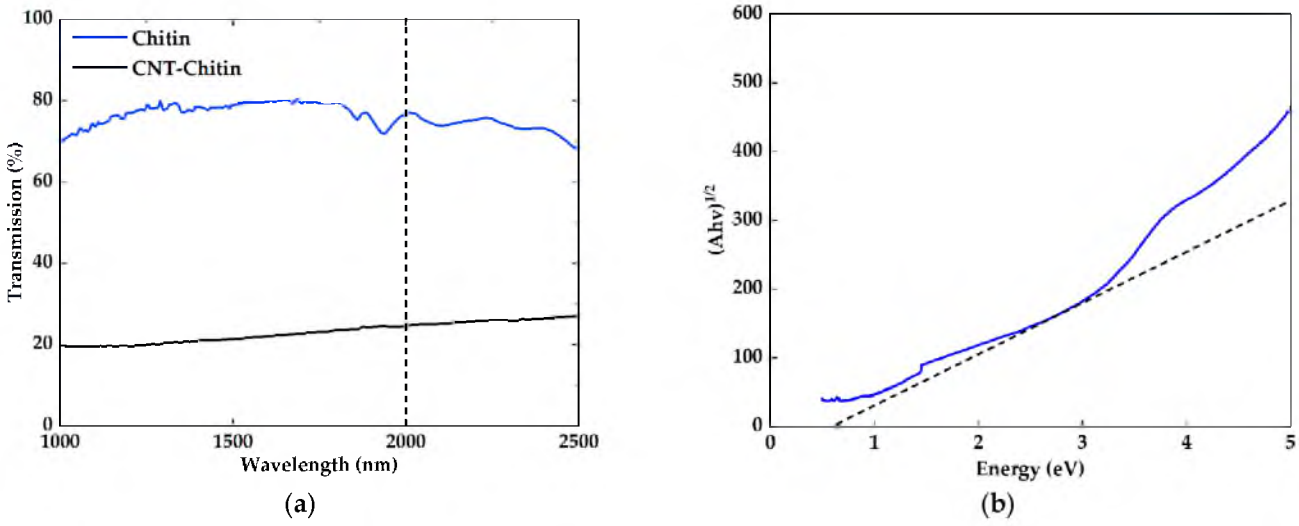

Figure 3. (**a**) Transmission spectrum and (**b**) Tauc relation of CNT–chitin film.

The nonlinear optical properties of the CNT-chitin were measured using power-dependent absorption measurement, as shown in Figure 4a. A mode-locked laser with a center wavelength of 1969 nm, which we constructed in-house, was used as the seed laser for the nonlinear measurement. The laser had a repetition rate and pulse width of 18.7 MHz and 1 ps, respectively. The output from the seed laser was attenuated using a variable optical attenuator. It was then split using a 3 dB optical coupler in which one of the ports was connected to the CNT-chitin SA and another to an optical power meter (OPM) as a reference. The output power of both of the detectors was recorded using OPMs as the attenuation value gradually decreased. The power-dependent absorption measurement was then calculated and fitted using a two-level SA model [3]:

$$\alpha(I) = \frac{\alpha_o}{1 + \frac{I}{I_{sat}}} + \alpha_{ns} \quad (2)$$

where $\alpha(I)$ is the intensity-dependent absorption coefficient, and α_o, α_{ns}, and I_{sat} are the saturable absorption (modulation depth), non-saturable absorption and saturation intensity, respectively. As we can see in Figure 4b, the modulation depth, non-saturable absorption, and saturation intensity of the SA were 16.2%, 79.8%, and 0.1257 kW/cm^2, respectively. The high value of non-saturable losses is attributed to the residual absorption of amorphous carbon, metal catalysts, and CNTs not resonant with the incident light. In addition, scattering from the residual bundles and unevenness of the CNT–chitin surface may also lead to an increase in non-saturable loss, which could weaken the performance of a mode-locked laser due to a higher threshold of mode-locked operation and lower output power [3,49]. The modulation depth of the fabricated CNT-chitin is comparable with that reported in past literature for CNT-based SAs. For example, the authors in reference [50] reported an 18% modulation depth using a polymer-free CNT-based SA. In other research, Popa et al. [51] integrated CNTs with a sodium-carboxymethylcellulose polymer and obtained a modulation depth of 17% with thickness of 30 µm. Yamashita et al. [52] suggested that the modulation depth could be enhanced by increasing the thickness of the SA at the expense of higher non-saturable loss, hence requiring a higher pump power threshold to initiate the mode-locking operation. Jeon et al. [53] stated that in an anomalous dispersion regime with

a dispersion smaller than -0.08 ps^2, a small modulation depth of 1.5% was sufficient to produce stable mode-locked pulses. The pulse width was observed to decrease from 1.81 ps to 910 fs as the modulation depth increased from 1.5% to 39.5%. In our case, the modulation depth value was still within the range suggested by reference [53]. Figure 4c shows the error bars for the CNT-chitin film's non-linear optical absorption experimental data. The error might potentially be due to the uncertainty of the laser power or the thickness or position of the sample. The average error was around 2%, indicating reliable nonlinear optical measurement.

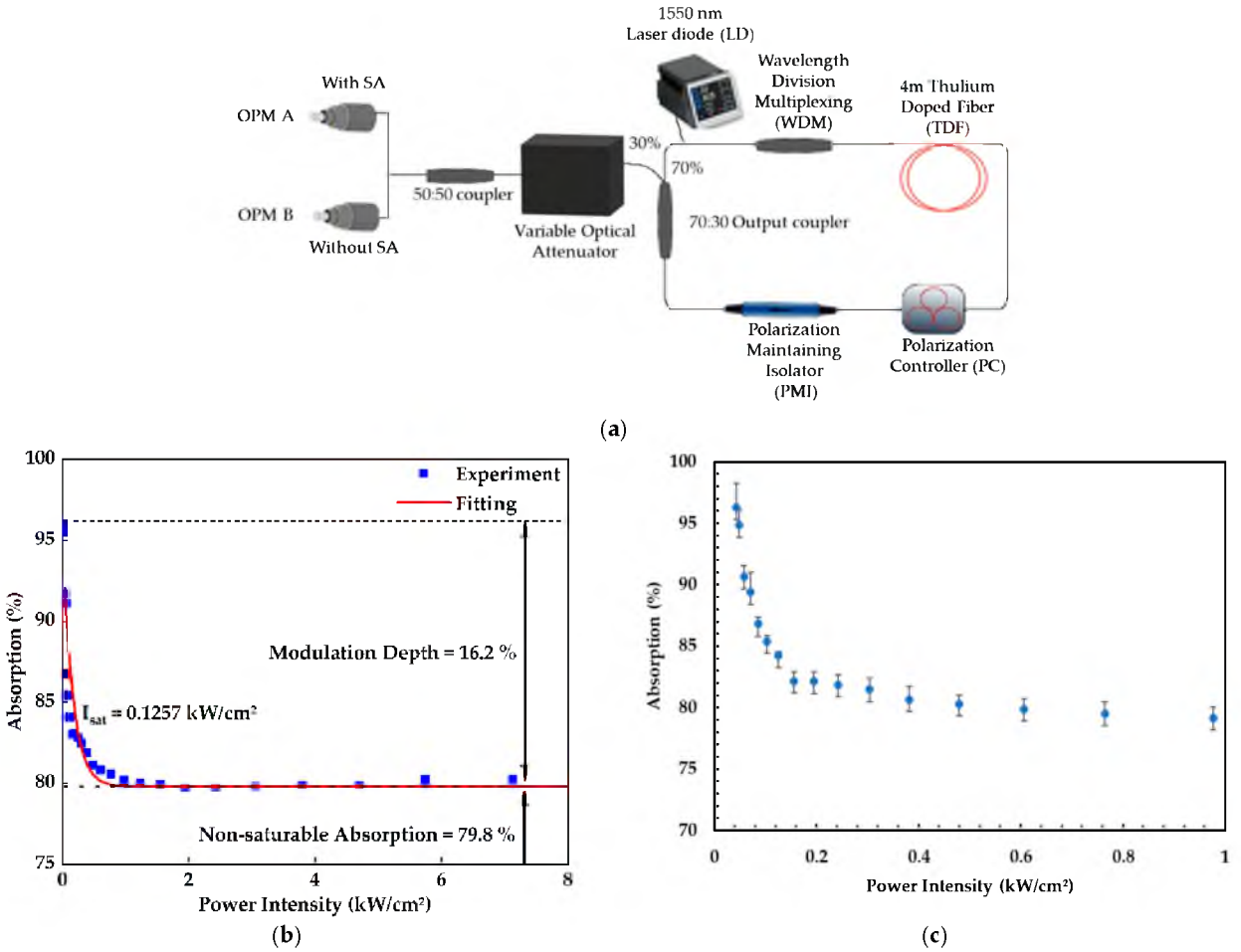

Figure 4. (**a**) Schematic diagram of power-dependent absorption measurement. (**b**) Non-linear optical absorption for CNT-chitin film. (**c**) Error bars for CNT-chitin film non-linear optical absorption experimental data.

2.3. Fiber Laser Setup

The experimental setup for the mode-locked THDFL is depicted in Figure 5. Two laser diodes (CLD1015, Thorlabs, Newton, NJ, USA) with 1550 nm center wavelengths were used to pump the gain medium, which was a 1.5 m highly doped thulium-holmium fibre. To maintain unidirectional laser operation, 1550 nm polarization-insensitive isolators (PI-ISO) were placed at both ends of the amplifier section. A 1550/2000 nm wavelength division multiplexer (WDM) was placed after each 1550 nm PI-ISO to guide the 1550 nm pumped light to the gain medium. A 2000 nm PI-ISO was placed after the WDM to allow the light to propagate only in the clockwise direction. The free-standing CNT-chitin SA (1 mm × 1 mm) was then sandwiched between two fibre ferrules inside a physical contact ferrule connector to form the mode-locker. Light was then extracted from the cavity using a 90/10 coupler. The THDFL cavity consisted of a 13 m single-mode fibre laser (SMF) and 1.5 m of THDF. The output signal was measured using a 500 MHz digital oscilloscope

(DLM 2054, Yokogawa, Tokyo, Japan) with a 12.5 GHz InGaAs photodetector (Newport, 818-BB-51F, Irvine, CA, USA), an optical spectrum analyzer (AQ6370, Yokogawa, Tokyo, Japan) with resolution of 0.2 nm, an optical power meter (PM100USB, Thorlabs, Newton, NJ, USA), an autocorrelator (PulseCheck 150, APE, Berlin, Germany), and a radio frequency spectrum analyzer (RFSA) (Rohde & Schwarz, FSC 6, Munich, Germany). This equipment was used to measure the pulse train, optical spectrum analyzer, output power, pulse width and signal-to-noise ratio (SNR) of the generated pulse, respectively. The cavity consisted of 1.5 m of THDF gain medium and about 13 m of SMF-28.The group velocity dispersion (GVD) of SMF-28 was calculated to be -0.0572 ps^2 m^{-1}, and the GVD of THDF was calculated to be -0.0563 ps^2 m^{-1} at 2.0 µm. The net cavity dispersion was calculated using the formula $L_{THDF}GVD_{THDF} + L_{SMF}GVD_{SMF}$ to obtain a value of -0.6596 ps^2.

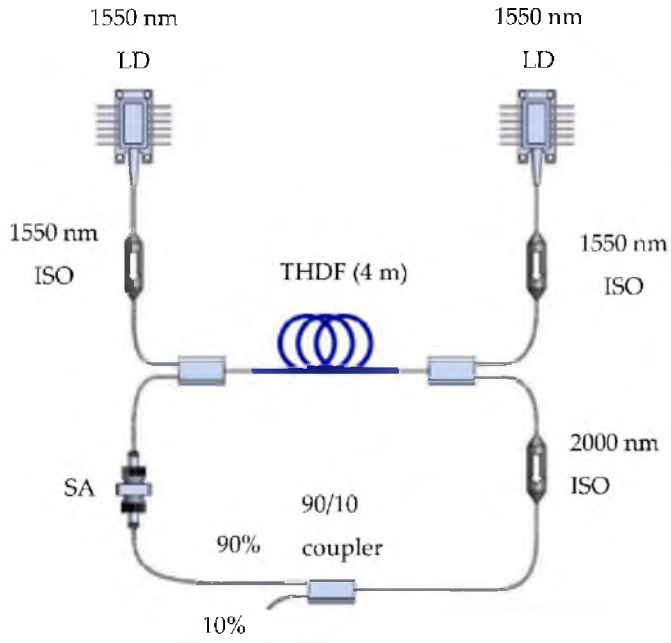

Figure 5. Schematic diagram of the mode-locked THDFL experimental setup. Adapted with permission from Ref. [28]. 2021, S. N. F. Zuikafly".

3. Results and Discussion

Figure 6 shows the performance of the mode-locking operation of the THDFL. The optical spectrum of the mode-locked THDFL obtained using CNTs embedded in chitin is shown in Figure 6a,b. The soliton mode-locking operation of the THDFL for CNT-chitin self-started at 203 mW pump power without the use of a polarization controller (PC), as shown in Figure 6a. The laser operated at maximum input power of 228.6 mW at a 1908.53 nm central wavelength with an output power of 0.4 mW and a 3 dB spectral bandwidth of 3.59 nm. The 3 dB bandwidth used here is less than that for CNT-carboxymethyl cellulose (CNT-CMC) SA [54], and comparable to the previous study using a CNT-based SA [55]. The presence of several pairs of Kelly sidebands was also observed in the spectrum, indicating that the laser operated in a soliton mode-locked regime in an anomalous dispersion region. The Kelly sidebands were formed due to the increase in the resonance effect between the solitons and the dispersive wave created by the pulse [56]. The soliton pulse was periodically disturbed by the linear effect of anomalous group delay dispersion and the nonlinear effect of self-phase modulation, which resulted in the appearance of the sidebands [55].

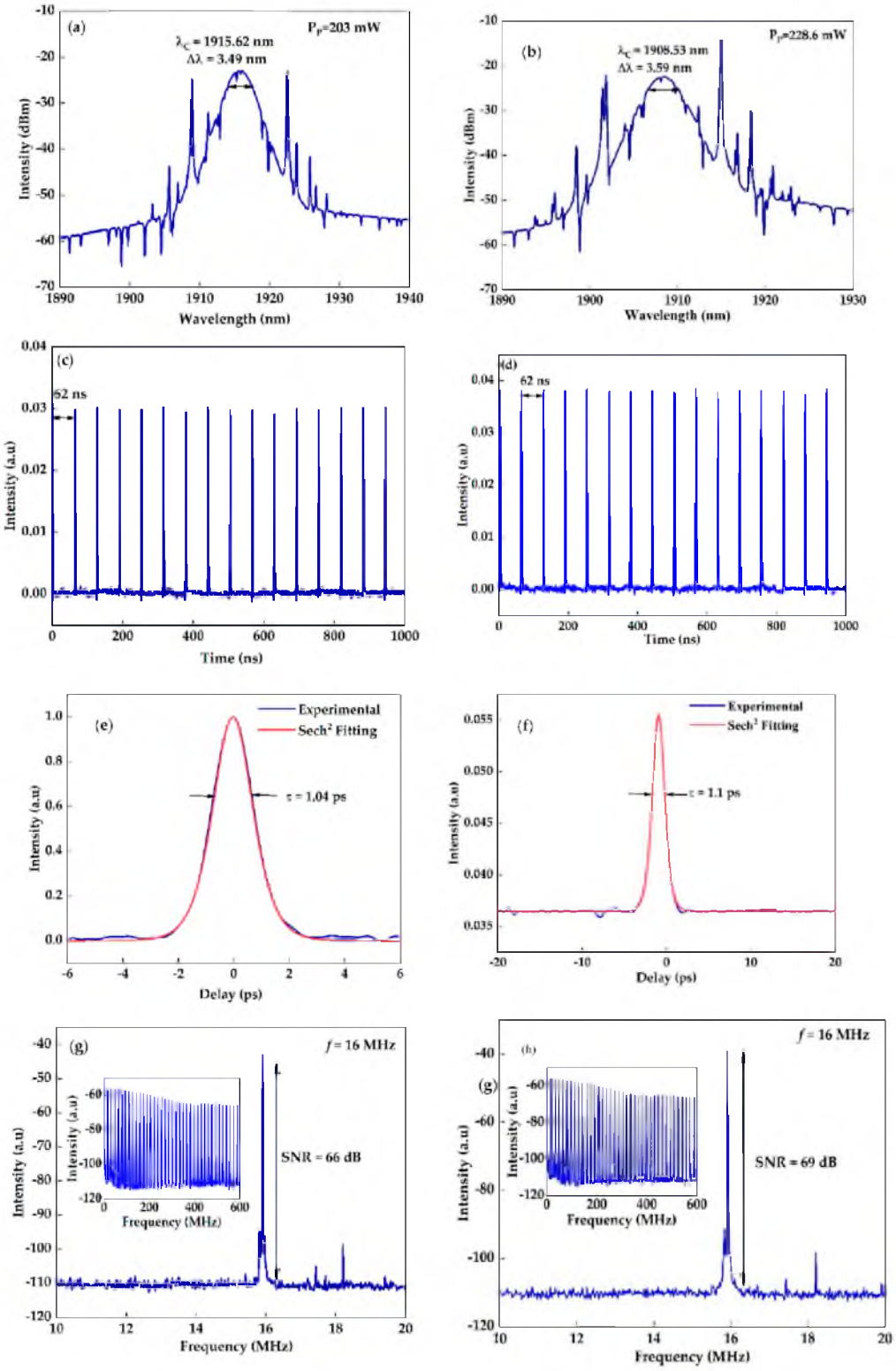

Figure 6. Performance of the mode-locking operation of THDFL at threshold and maximum pump power: (**a**,**b**) OSA trace; (**c**,**d**) Output pulse train with pulse-to-pulse separation of 62 ns; (**e**,**f**) Auto-correlation trace with pulse widths of 1.04 and 1.1 ps; (**g**,**h**) RFSA where SNR ratios at pump powers of 203 mW and 228.6 mW are 66 dB and 69 dB.

As depicted in Figure 6c,d, the mode-locking operation of the THDFL was further investigated by evaluating the pulse train. The pulse train had a pulse-to-pulse separation of 62 ns, corresponding to the repetition rate of 16 MHz. The absence of fluctuation of

the peaks in the pulse train indicated the non-existence of Q-switching modulation or instabilities in the mode-locked pulses. The repetition rate corresponded well to the actual cavity length of approximately 13 m and remained constant from 203 mW to 228.6 mW, confirming the fundamental characteristics of the mode-locking mechanism.

Figure 6e,f shows the pulse width of the CNT embedded in chitin, measured at around 1.1 ps. The pulse width in this study was shorter than that reported for carbon-based SAs such as CNT and graphene [28,57–59]. The figure also includes the $sech^2$ fitting, demonstrating the soliton pulse generation. The autocorrelation trace showed that the experimental result closely reflected the $sech^2$ fitting. The time-bandwidth product (TBP) was then calculated based on the formula given in Equation (3) below. The calculated TBP was 0.325, slightly higher than the transform-limited value of 0.315, which is the standard temporal profile of $sech^2$ pulses. The TBP value is comparable to carbon nanotube SAs as reported by other researchers [60–62]. The calculated TBP indicated the existence of a chirp pulse as in Equation (3) [63]:

$$TBP = \Delta t.\Delta\lambda\frac{c}{\lambda^2} \quad (3)$$

where Δt is the pulse width, λ is the central wavelength, c is the speed of light, and $\Delta\lambda$ is the 3-dB bandwidth of the mode-locked spectrum.

Figure 6g,h shows the RFSA spectrum of the mode-locked THDFL where signal-to-noise ratio (SNR) at the pump power of 203 mW and 228.6 mW are 66 dB and 69 dB. The spectra for both samples demonstrated that the mode-locked pulse at the fundamental frequency of 16 MHz was very stable. The value of the SNR achieved in this work was higher than the studies by previous researchers [50,64–66], in which the SNR value was less than 65 dB for CNT embedded in a synthetic host polymer, which indicates that CNT-chitin SA has very good potential for superior mode-locking operation when carefully employed in an appropriate laser system.

Table 1 summarizes the comparison of mode lockers with different material in the 2 μm region. Wang et al. [17] used CNT-PVA mode-locked Tm-doped fibre lasers with a total cavity length of ~120 m and a dispersion of ~−10.75 ps^2, obtaining stable mode-locked pulses with a pulse width of ~9.3 ns. Sobon et al. [50] reported on the performance of a mode-locked Tm-doped fibre laser using a CNT film. The CNTs were fabricated using a vacuum filtration technique and deposited on fibre connector end facets where a pulse width of 0.501 ps was obtained. The mode-locked laser of this work was able to generate significantly shorter pulse widths (1.1 ps) compared to other CNT-based SAs reported in references [17,50,55]. It is noted that the shorter pulse widths obtained could be attributed to the cavity working with a low anomalous net cavity dispersion. This can be confirmed by Zhang et al. [67], who demonstrated that when the anomalous dispersion value decreased, the pulse width value also decreased proportionally.

The TBP value for this study is lower than the TBP values reported in CNT and graphene-based SAs in Table 1. The threshold pump power used in this study is lower than the values reported in references [17,28,50,55,68–70]. Aside from the high nonlinear response of both CNT and graphene, which enhances the absorption of photons, the use of chitin in this case compared to other synthetic polymers reduces the pump power needed to achieve mode-locked operation due to its reduced saturation fluence, as chitin has low saturation intensity. Since it is known that the choice of host polymer can affect the packing density and orientation of the SA molecules, which in turn can affect the nonlinear optical response and saturation fluence, chitin can be said to be more compatible with the base material [28]. Furthermore, the SNR value of this work was 69 dB, which is high compared to those reported in references [17,28,50,63–65], suggesting that CNTs embedded in chitin can improve the performance of SAs in laser applications. The output power of the CNT-chitin saturable absorber is lower compared to other saturable absorbers listed in the tables. This value might be due to the samples' high value of non-saturable loss (79.8%). Higher non-saturable loss is attributed to the residual absorption of amorphous carbon, metal catalysts, and CNTs not resonant with the incident light. This leads to lower

output power for the CNT-chitin samples compared to others listed in Table 1. Output power can be enhanced by inserting an amplifier in the fire laser cavity, as in Zuikafly et al. [28]. However, it is worth stating that the previous papers vary in the reported form of output power between average or maximum output power, so a proper comparison is hard to make.

Overall, laser performance in this study was better than most if not all related previous studies, as shown in Table 1. This shows the potential of CNT-chitin-based SAs for multiple applications in the 2 µm region, such as medical surgery, free-space optical communications, light detection and ranging (LIDAR), nonlinear frequency conversion, and transparent material processing.

Table 1. Mode−Locker for SA in 2 µm region.

Material	Diameter of Material (nm)	Center Wave-length (nm)	Threshold Pump Power (mW)	Pulse Width (ps)	Repetition Rate (MHz)	SNR (dB)	TBP	Modulation Depth (%)	Average Output Power (mW)	Ref
SWCNT-PVA	-	2003.1	-	9300	1.718	63	~904	23.7	46	[17]
SWCNT (Polymer free)	1.4	1928.5	410	0.501	56.37	~70	0.343	13	28.5	[50]
CNT-SA with a diffraction grating mirror	~1.3–1.6	1960	240	2.43	18.4	>60	0.567	42.3	~1	[55]
SWCNT microfiber	-	1967.79	500	0.896	17.2	>57	0.318	16.5	6.54	[68]
SWCNT-Polyimide film	1.6	2000	-	0.211	21.4	66	-	10	36.1	[70]
Graphene-Chitin	-	1982.7	76.2	1.88	11.35	43	0.416	18.56	3.43	[28]
Graphene-PMMA	-	2060	1000	0.19	20.98	65	0.72	12	54	[69]
CNT–chitin	1–2	1908.53	203	1.1	16	69	0.325	16.7	0.4	This work

4. Conclusions

A mode-locked THDFL was proposed and demonstrated. A film of CNTs embedded in bio-polymer chitin as a host polymer was successfully fabricated as an SA and incorporated into the cavity. Mode-locking was observed at a central wavelength of 1908.53 nm with a spectral bandwidth of 3.59 nm and an output power of 0.4 mW. A stable pulse with a pulse width of 1.1 ps and a repetition rate of 16 MHz was observed. In summary, this work demonstrated a CNT embedded in chitin as an SA in the 2 µm region having enhanced mode-locking performance, while also using a bio-polymer as an alternative to synthetic polymers.

Author Contributions: Conceptualization, N.N.M.R., F.A. and S.N.F.Z.; methodology, F.A., H.A. and M.F.I.; validation, F.A., H.A. and M.F.I.; formal analysis, N.N.M.R., H.Y. and W.M.F.W.N.; investigation, N.N.M.R., F.A. and S.N.F.Z.; resources, H.A. and M.F.I.; data curation, N.N.M.R. and M.Q.L.; writing—original draft preparation, N.N.M.R. and S.N.F.Z.; writing—review and editing, F.A. and S.N.F.Z.; visualization, N.A.N., W.M.F.W.N. and H.Y.; supervision, F.A. and N.A.N.; project administration, F.A.; funding acquisition, F.A. All authors have read and agreed to the published version of the manuscript.

Funding: This research was funded by UTM R&D Fund Tier 2, grant number 17J24 and UTM High Impact Research, grant number 08G99.

Institutional Review Board Statement: Not applicable.

Informed Consent Statement: Not applicable.

Data Availability Statement: Not applicable.

Acknowledgments: The authors would like to acknowledge Malaysia-Japan International Institute of Technology (MJIIT), Universiti Teknologi Malaysia and Photonics Research Centre, University of Malaya, for providing facility and equipment throughout this project. M.Q.L. and S.N.F.Z. also would like to thank Universiti Teknologi Malaysia for Postdoctoral Fellowships.

Conflicts of Interest: The authors declare no conflict of interest.

References

1. Yu, Z.; Wang, Y.; Zhang, X.; Dong, X.; Tian, J.; Song, Y. A 66 fs highly stable single wall carbon nanotube mode locked fiber laser. *Laser Phys.* **2013**, *24*, 015105. [CrossRef]
2. Chernysheva, M.; Rozhin, A.; Fedotov, Y.; Mou, C.; Arif, R.; Kobtsev, S.M.; Dianov, E.M.; Turitsyn, S.K. Carbon nanotubes for ultrafast fibre lasers. *Nanophotonics* **2017**, *6*, 1–30. [CrossRef]
3. Wang, F.; Rozhin, A.G.; Scardaci, V.; Sun, Z.; Hennrich, F.; White, I.H.; Milne, W.I.; Ferrari, A.C. Wideband-tuneable, nanotube mode-locked, fibre laser. *Nat. Nanotechnol.* **2008**, *3*, 738–742. [CrossRef] [PubMed]
4. Reich, S.; Thomsen, C.; Maultzsch, J. *Carbon Nanotubes: Basic Concepts and Physical Properties*; Wiley & Sons: Hoboken, NJ, USA, 2007.
5. Set, S.Y.; Yaguchi, H.; Tanaka, Y.; Jablonski, M.; Sakakibara, Y.; Rozhin, A.; Tokumoto, M.; Kataura, H.; Achiba, Y.; Kikuchi, K. Mode-locked fiber lasers based on a saturable absorber incorporating carbon nanotubes. In Proceedings of the Conference on Optical Fiber Communication, Atlanta, GA, USA, 28 March 2003; IEEE: Piscataway, NJ, USA, 2003.
6. Cheng, D.; Yan, F.; Feng, T.; Bai, Z.; Zhang, L.; Wang, W.; Liu, S.; Zhou, H.; Hou, Y. Single weakly tilted FBG in 2-μm band capable of measuring temperature, axial strain, and surrounding refractive index. *Opt. Eng.* **2018**, *57*, 096107. [CrossRef]
7. Geng, J.; Wang, Q.; Lee, Y.; Jiang, S. Development of Eye-Safe Fiber Lasers Near 2 μm. *IEEE J. Sel. Top. Quantum Electron.* **2014**, *20*, 150–160. [CrossRef]
8. Scholle, K.; Lamrini, S.; Koopmann, P.; Fuhrberg, P. 2 μm Laser Sources and Their Possible Applications. In *Frontiers in Guided Wave Optics and Optoelectronics*; IntechOpen: London, UK, 2010.
9. Cao, R.; Lu, Y.; Tian, Y.; Huang, F.; Xu, S.; Zhang, J. Spectroscopy of thulium and holmium co-doped silicate glasses. *Opt. Mater. Express* **2016**, *6*, 2252–2263. [CrossRef]
10. Kieu, K.; Wise, F.W. Soliton thulium-doped fiber laser with carbon nanotube saturable absorber. *IEEE Photonics Technol. Lett.* **2009**, *21*, 128–130. [CrossRef]
11. Kivistö, S.; Hakulinen, T.; Kaskela, A.; Aitchison, B.; Brown, D.P.; Nasibulin, A.G.; Kauppinen, E.I.; Härkönen, A.; Okhotnikov, O.G. Carbon nanotube films for ultrafast broadband technology. *Opt. Express* **2009**, *17*, 2358–2363. [CrossRef]
12. Huang, B. Carbon nanotubes and their polymeric composites: The applications in tissue engineering. *Biomanuf. Rev.* **2020**, *5*, 3. [CrossRef]
13. Nurazzi, N.M.; Asyraf, M.R.M.; Khalina, A.; Abdullah, N.; Sabaruddin, F.A.; Kamarudin, S.H.; Ahmad, S.; Mahat, A.M.; Lee, C.L.; Aisyah, H.A.; et al. Fabrication, Functionalization, and Application of Carbon Nanotube-Reinforced Polymer Composite: An Overview. *Polymers* **2021**, *13*, 1047. [CrossRef]
14. Ahmad, H.; Sharbirin, A.S.; Ismail, M.F. 1.8 μm passively Q-switched thulium-doped fiber laser. *Opt. Laser Technol.* **2019**, *120*, 105757. [CrossRef]
15. Harun, S.W.; Saidin, N.; Zen, D.I.M.; Ali, N.M.; Ahmad, H.; Ahmad, F.; Dimyati, K. Self-starting harmonic mode-locked thulium-doped fiber laser with carbon nanotubes saturable absorber. *Chin. Phys. Lett.* **2013**, *30*, 094204. [CrossRef]
16. Wu, K.; Zhang, X.; Wang, J.; Chen, J. 463-MHz fundamental mode-locked fiber laser based on few-layer MoS_2 saturable absorber. *Opt. Lett.* **2015**, *40*, 1374–1377. [CrossRef]
17. Wang, M.; Huang, Y.; Song, Z.; Wei, J.; Pei, J.; Ruan, S. Two-micron all-fiberized passively mode-locked fiber lasers with high-energy nanosecond pulse. *High Power Laser Sci. Eng.* **2020**, *8*, e14. [CrossRef]
18. Ahmad, H.; Samion, M.Z.; Sharbirin, A.S.; Norizan, S.F.; Aidit, S.N.; Ismail, M.F. Graphene-PVA saturable absorber for generation of a wavelength-tunable passively Q-switched thulium-doped fiber laser in 2.0 μm. *Laser Phys.* **2018**, *28*, 055105. [CrossRef]
19. Xu, N.; Yang, W.; Zhang, H. Nonlinear saturable absorption properties of indium selenide and its application for demonstrating a Yb-doped mode-locked fiber laser. *Opt. Mater. Express* **2018**, *8*, 3092–3103. [CrossRef]
20. Aziz, S.B.; Nofal, M.M.; Brza, M.A.; Hussein, S.A.; Mahmoud, K.H.; El-Bahy, Z.M.; Dannoun, E.M.A.; Kareem, W.O.; Hussein, A.M. Characteristics of PEO Incorporated with $CaTiO_3$ Nanoparticles: Structural and Optical Properties. *Polymers* **2021**, *11*, 13. [CrossRef]
21. Abdelrazek, E.M.; Abdelghany, A.M.; Badr, S.I.; Morsi, M.A. Structural, optical, morphological and thermal properties of PEO/PVP blend containing different concentrations of biosynthesized Au nanoparticles. *J. Mater. Res. Technol.* **2018**, *7*, 419–431. [CrossRef]
22. Ngai, K.S.; Ramesh, S.; Ramesh, K.; Juan, J.C. A review of polymer electrolytes: Fundamental, approaches and applications. *Ionics* **2016**, *22*, 1259–1279. [CrossRef]

23. Muhammed, D.S.; Brza, M.A.; Nofal, M.M.; Aziz, S.B.; Hussen, S.A.; Abdulwahid, R.T. Optical Dielectric Loss as a Novel Approach to Specify the Types of Electron Transition: XRD and UV-vis as a Non-Destructive Techniques for Structural and Optical Characterization of PEO Based Nanocomposites. *Materials* **2020**, *13*, 2979. [CrossRef]
24. Luo, Z.; Li, Y.; Zhong, M.; Huang, Y.; Wan, X.; Peng, J.; Weng, J. Nonlinear optical absorption of few-layer molybdenum diselenide ($MoSe_2$) for passively mode-locked soliton fiber laser. *Photonics Res.* **2015**, *3*, 79–86. [CrossRef]
25. Jayakumar, R.; Rani, V.D.; Shalumon, K.T.; Kumar, P.T.; Nair, S.V.; Furuike, T.; Tamura, H. Bioactive and osteoblast cell attachment studies of novel α-and β-chitin membranes for tissue-engineering applications. *Int. J. Biol. Macromol.* **2009**, *45*, 260–264. [CrossRef] [PubMed]
26. Elieh-Ali-Komi, D.; Hamblin, M.R. Chitin and Chitosan: Production and Application of Versatile Biomedical Nanomaterials. *Int. J. Adv. Res.* **2016**, *4*, 411–427.
27. Shervani, Z. Chitin-gold nanocomposite film and electro-optical properties. *Front. Nanosci. Nanotechnol.* **2017**, *3*, 2–4. [CrossRef]
28. Zuikafly, S.N.F.; Ahmad, H.; Nawawi, W.M.F.W.; Yahaya, H.; Ibrahim, M.H.; Latif, A.A.; Ahmad, F. Graphene-chitin bio-composite polymer based mode locker at 2 micron region. *Optik* **2021**, *245*, 167710. [CrossRef]
29. Goh, S.X.L.; Goh, E.X.Y.; Lee, H.K. Sodium dodecyl sulfate-multi-walled carbon nanotubes-coated-membrane solid phase extraction of glucocorticoids in aqueous matrices. *Talanta* **2021**, *221*, 121624. [CrossRef]
30. Vaisman, L.; Wagner, H.D.; Marom, G. The role of surfactants in dispersion of carbon nanotubes. *Adv. Colloid Interface Sci.* **2006**, *21*, 128–130. [CrossRef]
31. Yu, J.; Grossiord, N.; Koning, C.E.; Loos, J. Controlling the dispersion of multi-wall carbon nanotubes in aqueous surfactant solution. *Carbon* **2007**, *45*, 618–623. [CrossRef]
32. Strano, M.S.; Moore, V.C.; Miller, M.K.; Allen, M.J.; Haroz, E.H.; Kittrell, C.; Hauge, R.H.; Smalley, R.E. The role of surfactant adsorption during ultrasonication in the dispersion of single-walled carbon nanotubes. *J. Nanosci. Nanotechnol.* **2003**, *3*, 81–86. [CrossRef]
33. Fazli Wan Nawawi, W.M.; Lee, K.Y.; Kontturi, E.; Murphy, R.J.; Bismarck, A. Chitin Nanopaper from Mushroom Extract: Natural Composite of Nanofibers and Glucan from a Single Biobased Source. *ACS Sustain. Chem. Eng.* **2019**, *7*, 6492–6496. [CrossRef]
34. Jorio, A.; Pimenta, M.A.; Souza Filho, A.G.; Saito, R.; Dresselhaus, G.; Dresselhaus, M.S. Characterizing carbon nanotube samples with resonance Raman scattering. *New J. Phys.* **2003**, *5*, 139. [CrossRef]
35. Villalpando-Paez, F.; Son, H.; Nezich, D.; Hsieh, Y.P.; Kong, J.; Kim, Y.A.; Shimamoto, D.; Muramatsu, H.; Hayashi, T.; Endo, M.; et al. Raman spectroscopy study of isolated double-walled carbon nanotubes with different metallic and semiconducting configurations. *Nano Lett.* **2008**, *8*, 3879–3886. [CrossRef]
36. Shea, M.J.; Wall, M.H. Representative raman measurements of carbon nanotubes. *Spectrosc. Eur.* **2012**, *24*, 14–16.
37. Martinez, A.; Sun, Z. Nanotube and graphene saturable absorbers for fibre lasers. *Nat. Photonics* **2013**, *7*, 842–845. [CrossRef]
38. Ahmad, F.; Harun, S.W.; Nor, R.M.; Zulkepely, N.R.; Ahmad, H.; Shum, P. A passively mode-locked erbium-doped fiber laser based on a single-wall carbon nanotube polymer. *Chin. Phys. Lett.* **2013**, *30*, 054210. [CrossRef]
39. Tarka, J.; Sobon, G.; Boguslawski, J.; Sotor, J.; Jagiello, J.; Aksienionek, M.; Lipinska, L.; Zdrojek, M.; Judek, J.; Abramski, K.M. 168 fs pulse generation from graphene-chitosan mode-locked fiber laser. *Opt. Mater. Express* **2014**, *4*, 1981–1986. [CrossRef]
40. Zhang, M.; Hu, G.; Hu, G.; Howe, R.C.; Chen, L.; Zheng, Z.; Hasan, T. Yb- and Er-doped fiber laser Q-switched with an optically uniform, broadband WS2 saturable absorber. *Sci. Rep.* **2015**, *5*, 17482. [CrossRef]
41. Lau, K.Y.; Liu, X.; Qiu, J. Comparison for Saturable Absorbers: Carbon Nanotube Versus Graphene. *Adv. Photonics Res.* **2022**, *3*, 2200023. [CrossRef]
42. Liu, H.H.; Chow, K.K.; Yamashita, S.; Set, S.Y. Carbon-nanotube-based passively Q-switched fiber laser for high energy pulse generation. *Opt. Laser Technol.* **2013**, *45*, 713–716. [CrossRef]
43. Cheng, K.N.; Lin, Y.H.; Lin, G.R. Single- and double-walled carbon nanotube based saturable absorbers for passive mode-locking of an erbium-doped fiber laser. *Laser Phys.* **2013**, *23*, 045105. [CrossRef]
44. Liu, K.; Deslippe, J.; Xiao, F.; Capaz, R.B.; Hong, X.; Aloni, S.; Zettl, A.; Wang, W.; Bai, X.; Louie, S.G.; et al. An atlas of carbon nanotube optical transitions. *Nat. Nanotechnol.* **2012**, *7*, 325–329. [CrossRef] [PubMed]
45. Hasan, T.; Sun, Z.; Tan, P.; Popa, D.; Flahaut, E.; Kelleher, E.J.; Bonaccorso, F.; Wang, F.; Jiang, Z.; Torrisi, F.; et al. Double-wall carbon nanotubes for wide-band, ultrafast pulse generation. *ACS Nano* **2014**, *8*, 4836–4847. [CrossRef] [PubMed]
46. Halim, S.N.M.; Ahmad, F.; Lokman, M.Q.; Sapingi, H.H.J.; Taib, M.F.M.; Nawawi, W.M.F.W.; Yahaya, H.; Rahman, M.A.A.; Shafie, S.; Harun, S.W. First Principles Study and Experimental Investigation of Graphene-Molybdenum Disulphide Nanocomposites Based Passive Saturable Absorber. *Photonics* **2022**, *9*, 704. [CrossRef]
47. Geng, H.Z.; Lee, D.S.; Kim, K.K.; Han, G.H.; Park, H.K.; Lee, Y.H. Absorption spectroscopy of surfactant-dispersed carbon nanotube film: Modulation of electronic structures. *Chem. Phys. Lett.* **2008**, *455*, 275–278. [CrossRef]
48. Apandi, N.M.; Ahmad, H.; Lokman, M.Q.; Zuikafly, S.N.F.; Yahaya, H.; Ibrahim, M.H.; Rosnan, R.M.; Ahmad, F. Observation of soliton and bound soliton in erbium-doped fiber lasers using single-walled carbon nanotubes mode-lockers under gamma irradiation. *Opt. Laser Technol.* **2023**, *157*, 108775. [CrossRef]
49. Dai, L.; Huang, Z.; Huang, Q.; Zhao, C.; Rozhin, A.; Sergeyev, S.; Al Araimi, M.; Mou, C. Carbon nanotube mode-locked fiber lasers: Recent progress and perspectives. *Nanophotonics* **2021**, *10*, 749–775. [CrossRef]
50. Sobon, G.; Duzynska, A.; Świniarski, M.; Judek, J.; Sotor, J.; Zdrojek, M. CNT-based saturable absorbers with scalable modulation depth for Thulium-doped fiber lasers operating at 1.9 µm. *Sci. Rep.* **2017**, *7*, 45491. [CrossRef]

51. Popa, D.; Sun, Z.; Hasan, T.; Cho, W.; Wang, F.; Torrisi, F.; Ferrari, A.C. 74-fs nanotube-mode-locked fiber laser. *Appl. Phys. Lett.* **2012**, *101*, 153107. [CrossRef]
52. Yamashita, S.; Martinez, A.; Xu, B. Short pulse fiber lasers mode-locked by carbon nanotubes and graphene. *Opt. Fiber Technol.* **2014**, *20*, 702–713. [CrossRef]
53. Jeon, J.; Lee, J.; Lee, J.H. Numerical study on the minimum modulation depth of a saturable absorber for stable fiber laser mode locking. *JOSA B* **2015**, *32*, 31–37. [CrossRef]
54. Wang, J.; Liang, X.; Hu, G.; Zheng, Z.; Lin, S.; Ouyang, D.; Wu, X.; Yan, P.; Ruan, S.; Sun, Z.; et al. 152 fs nanotube-mode-locked thulium-doped all-fiber laser. *Sci. Rep.* **2016**, *6*, 28885. [CrossRef]
55. Meng, Y.; Li, Y.; Xu, Y.; Wang, F. Carbon Nanotube Mode-Locked Thulium Fiber Laser With 200 nm Tuning Range. *Sci. Rep.* **2017**, *7*, 45109. [CrossRef]
56. Li, Y.; Gao, L.; Huang, W.; Gao, C.; Liu, M.; Zhu, T. All-fiber mode-locked laser via short single-wall carbon nanotubes interacting with evanescent wave in photonic crystal fiber. *Opt. Express* **2016**, *24*, 23450–23458. [CrossRef]
57. Lin, Y.H.; Lin, G.R. Kelly sideband variation and self four-wave-mixing in femtosecond fiber soliton laser mode-locked by multiple exfoliated graphite nano-particles. *Laser Phys. Lett.* **2013**, *10*, 045109. [CrossRef]
58. Lau, K.Y.; Zulkifli, M.Z. 1.56 μm and 1.93 μm synchronized mode-locked fiber laser with graphene saturable absorber. *Infrared Phys. Technol.* **2021**, *112*, 103606. [CrossRef]
59. Wang, X.F.; Zhang, J.H.; Peng, X.L.; Mao, X.F. Generation and evolution of multiple operation states in passively mode-locked thulium-doped fiber laser by using a graphene-covered-microfiber. *Chin. Phys. B* **2018**, *27*, 084215. [CrossRef]
60. Dai, R.; Meng, Y.; Li, Y.; Qin, J.; Zhu, S.; Wang, F. Nanotube mode-locked, wavelength and pulsewidth tunable thulium fiber laser. *Opt. Express* **2019**, *27*, 3518–3527. [CrossRef]
61. Li, D.; Jussila, H.; Wang, Y.; Hu, G.; Albrow-Owen, T.C.T.; Howe, R.; Ren, Z.; Bai, J.; Hasan, T.; Sun, Z. Wavelength and pulse duration tunable ultrafast fiber laser mode-locked with carbon nanotubes. *Sci. Rep.* **2018**, *8*, 2738. [CrossRef]
62. Pawliszewska, M.; Dużyńska, A.; Zdrojek, M.; Sotor, J. Metallic carbon nanotube-based saturable absorbers for holmium-doped fiber lasers. *Opt. Express* **2019**, *27*, 11361–11369. [CrossRef]
63. Ahmad, H.; Sharbirin, A.S.; Muhamad, A.; Samion, M.Z.; Ismail, M.F. 2 μm mode-locked thulium-doped fiber laser using Mach-Zehnder interferometer tuning capability. *Laser Phys.* **2017**, *27*, 065104. [CrossRef]
64. Li, Y.; Yin, K.; Zhang, X.; Zheng, X.; Cheng, X.; Jiang, T. All-Fiber Bidirectional Mode-Locked Ultrafast Fiber Laser at 2 μm. *IEEE Photonics J.* **2019**, *11*, 7105708. [CrossRef]
65. Chen, Y.; Zhai, J.; Xu, X.; Li, L.; Wang, J.; Zhang, M.; Ruan, S.; Tang, Z. Mode-locked thulium-doped fiber laser based on 0.3 nm diameter single-walled carbon nanotubes at 1.95 μm. *Chin. Opt. Lett.* **2017**, *15*, 041403. [CrossRef]
66. Jiang, K.; Wu, Z.; Fu, S.; Song, J.; Li, H.; Tang, M.; Shum, P.; Liu, D. Switchable dual-wavelength mode-locking of thulium-doped fiber laser based on SWNTs. *IEEE Photonics Technol. Lett.* **2016**, *28*, 2019–2022. [CrossRef]
67. Zhang, L.; El-Damak, A.R.; Feng, Y.; Gu, X. Experimental and numerical studies of mode-locked fiber laser with large normal and anomalous dispersion. *Opt. Express* **2013**, *21*, 12014–12021. [CrossRef]
68. Li, Y.; Du, L.; Li, X.; Tao, Z.; Ma, W.; Wang, T.; Lou, Y.; Jiang, H. Noise-Like Pulse Generated by All-Fiber Ultrafast Thulium-Doped Fiber Laser Based on Single-Wall Carbon Nanotubes. *IEEE Photonics J.* **2022**, *14*, 7122905. [CrossRef]
69. Pawliszewska, M.; Martynkien, T.; Przewłoka, A.; Sotor, J. Dispersion-managed Ho-doped fiber laser mode-locked with a graphene saturable absorber. *Opt. Lett.* **2018**, *43*, 38–41. [CrossRef]
70. Watanabe, K.; Zhou, Y.; Saitoh, A.; Sakakibara, Y.; Nishizawa, N. Dispersion Managed, High Power TM-Doped Ultrashort Pulse Fiber Laser at 1.9 UM Using Single Wall Carbon Nanotube Polyimide Film. In Proceedings of the 2019 Conference on Lasers and Electro-Optics, CLEO, San Jose, CA, USA, 5–10 May 2019.